The Influence of Climate Feedbacks on Regional Hydrological Changes Under Global Warming

David B. Bonan[1] , Nicole Feldl[2] , Nicholas Siler[3] , Jennifer E. Kay[4,5] , Kyle C. Armour[6,7] , Ian Eisenman[8] , and Gerard H. Roe[9]

[1]Environmental Science and Engineering, California Institute of Technology, Pasadena, CA, USA, [2]Earth and Planetary Sciences, University of California Santa Cruz, Santa Cruz, CA, USA, [3]College of Earth, Ocean, and Atmospheric Sciences, Oregon State University, Corvallis, OR, USA, [4]Department of Atmospheric and Oceanic Sciences, University of Colorado, Boulder, CO, USA, [5]Cooperative Institute for Research in Environmental Sciences, University of Colorado, Boulder, CO, USA, [6]Department of Atmospheric Sciences, University of Washington, Seattle, WA, USA, [7]School of Oceanography, University of Washington, Seattle, WA, USA, [8]Scripps Institution of Oceanography, University of California San Diego, La Jolla, CA, USA, [9]Department of Earth and Space Sciences, University of Washington, Seattle, WA, USA

Abstract The influence of climate feedbacks on regional hydrological changes under warming is poorly understood. Here, a moist energy balance model (MEBM) with a Hadley Cell parameterization is used to isolate the influence of climate feedbacks on changes in zonal-mean precipitation-minus-evaporation ($P - E$) under greenhouse-gas forcing. It is shown that cloud feedbacks act to narrow bands of tropical $P - E$ and increase $P - E$ in the deep tropics. The surface-albedo feedback shifts the location of maximum tropical $P - E$ and increases $P - E$ in the polar regions. The intermodel spread in the $P - E$ changes associated with feedbacks arises mainly from cloud feedbacks, with the lapse-rate and surface-albedo feedbacks playing important roles in the polar regions. The $P - E$ change associated with cloud feedback locking in the MEBM is similar to that of a climate model with inactive cloud feedbacks. This work highlights the unique role that climate feedbacks play in causing deviations from the "wet-gets-wetter, dry-gets-drier" paradigm.

Plain Language Summary Climate feedbacks, which act to amplify or dampen global warming, play an important role in shaping how the climate system responds to changes in greenhouse-gas concentrations. Here, we use an idealized climate model, which makes a simplified assumption about how energy is transported in the atmosphere, to examine how climate feedbacks influence the patterns of precipitation and evaporation change under global warming. We find that the cloud feedback acts to narrow the band of rainfall on the equator known as the Intertropical Convergence Zone and that the surface-albedo feedback acts to shift the location of maximum rainfall. We also find that the cloud feedback accounts for most of the uncertainty associated with feedbacks in regional hydrological change under warming. The idealized model with a locked cloud feedback also simulates a change in precipitation and evaporation that is similar to a comprehensive climate model with an inactive cloud feedback.

1. Introduction

Climate feedbacks, which govern the top-of-atmosphere (TOA) radiative response to surface warming, have long been known to play a central role in shaping the climate response to forcing (e.g., Charney et al., 1979; Hansen et al., 1984). In recent years, climate feedbacks have been used to explain why climate models, when subject to increased greenhouse-gas concentrations, exhibit a large intermodel spread in global-mean surface temperature change (Cess & Potter, 1987; Cess et al., 1989; Dufresne & Bony, 2008; Roe & Baker, 2007; Soden & Held, 2006; Webb et al., 2013; Zelinka et al., 2020) and in other features, such as Arctic amplification (Beer & Eisenman, 2022; Bonan et al., 2018; Goosse et al., 2018; Hahn et al., 2021; Pithan & Mauritsen, 2014; Roe et al., 2015; Stuecker et al., 2018). It is argued that cloud feedbacks are the dominant contributor to uncertainty in warming at both regional (e.g., Bonan et al., 2018) and global (e.g., Dufresne & Bony, 2008; Soden & Held, 2006; Zelinka et al., 2020) scales.

While it is clear that climate feedbacks exert a strong influence on surface temperature change, it is less clear what influence they have on other components of the climate system, such as regional hydrological changes. Recent studies have linked regional hydrological changes to the atmospheric energy budget and climate feedbacks (Anderson et al., 2018; Bonan, Feldl, et al., 2023; Muller & O'Gorman, 2011; Pithan & Jung, 2021). These studies

have found that dry-static energy transport shapes hydrological change in the tropics and that both dry-static energy transport and radiation together shape hydrological change in the polar regions. Bonan, Feldl, et al. (2023) further examined how radiative (or climate) feedbacks shape the pattern of precipitation change and found that in the polar regions, the Planck feedback exerts a strong control on atmospheric radiative cooling and thus precipitation increases. However, such diagnostic approaches hinder inference about how radiative processes in one region affect the hydrological response in another. Quantifying the influence of radiative feedbacks on regional hydrological change requires using a framework that enables feedbacks and atmospheric energy transport to interact with each other across latitudes (e.g., Merlis, 2014).

Several recent studies have shown that regional hydrological change can be understood through the lens of downgradient atmospheric energy transport, which provides a framework for quantifying the role of local and nonlocal radiative processes (Armour et al., 2019; Bonan, Siler, et al., 2023; Siler et al., 2018). Siler et al. (2018) used a moist energy balance model (MEBM) to connect the change in precipitation-minus-evaporation ($P - E$) to downgradient atmospheric energy transport and showed that this perspective improved on the "wet-gets-wetter, dry-gets-drier" thermodynamic scaling of Held and Soden (2006). Additional work by Bonan, Siler, et al. (2023) showed that the pattern of radiative feedbacks places a strong energetic constraint on the atmosphere and can significantly alter the pattern of $P - E$ change. A less-negative net radiative feedback in the tropics results in a larger increase in tropical $P - E$ because the atmosphere cannot radiate sufficient energy away locally and must export energy to regions where radiative energy loss is more efficient (such as the subtropics). This increased energy export requires an increase in the strength of the Hadley circulation in the deep tropics and thus causes an increase in tropical $P - E$ via increased equator-ward moisture transport. However, it is unclear which radiative feedbacks are most responsible for causing changes to the Hadley circulation and thus the pattern of tropical $P - E$. It is also unclear how radiative feedbacks influence $P - E$ change in other regions, such as the extratropics, where feedbacks and atmospheric energy transport are tightly coupled (Feldl et al., 2017; Hwang & Frierson, 2010; Hwang et al., 2011). This leads to a key question: How do individual climate feedbacks influence the response of regional $P - E$ to warming?

The purpose of this paper is to investigate how individual radiative feedbacks modulate the response of zonal-mean $P - E$ to global warming. To do this, we use a MEBM with a Hadley Cell parameterization and output from climate models participating in Phase 5 of the Coupled Model Inter-comparison Project (CMIP5; Taylor et al., 2012). Our work combines the energetic perspective on regional precipitation change from Muller and O'Gorman (2011) with the energy transport perspective on regional hydrological changes from Siler et al. (2018) using a feedback-locking approach similar to Beer and Eisenman (2022). In what follows, we first describe the MEBM. We then remove individual radiative feedbacks in the MEBM and examine the influence of each on zonal-mean $P - E$ change. Our work shows that individual climate feedbacks can substantially modulate the "wet-gets-wetter, dry-gets-drier" paradigm that is commonly applied to understanding $P - E$ change under greenhouse-gas forcing via changes in atmospheric energy transport and feedback interactions. Finally, we compare feedback locking in the MEBM to feedback locking in a comprehensive climate model.

2. Methods

2.1. Moist Energy Balance Model (MEBM)

We simulate the change in zonal-mean near-surface air temperature T' and $P' - E'$ using a MEBM, which has been shown to accurately simulate patterns of temperature and hydrological change under greenhouse-gas forcing (e.g., Armour et al., 2019; Bonan et al., 2018; Bonan, Siler, et al., 2023; Feldl & Merlis, 2021; Flannery, 1984; Hwang & Frierson, 2010; Merlis & Henry, 2018; Peterson & Boos, 2020; Roe et al., 2015; Siler et al., 2018). The MEBM assumes that the change in poleward atmospheric energy transport F' is proportional to the change in the meridional gradient of near-surface moist static energy $h' = c_p T' + L_v q'$, where c_p is the specific heat of air (1,005 J kg^{-1} K^{-1}), L_v is the latent heat of vapourization (2.5×10^6 J kg^{-1}), and q' is the change in near-surface specific humidity (assuming fixed relative humidity of 80%). This gives

$$F' = \frac{2\pi p_s}{g} D\left(1 - x^2\right) \frac{dh'}{dx}, \tag{1}$$

where p_s is surface air pressure (1,000 hPa), g is the acceleration due to gravity (9.81 m s^{-2}), D is a constant diffusion coefficient (with units of m^2 s^{-1}), x is the sine of the latitude, and $1 - x^2$ accounts for the spherical geometry.

Under warming, the change in annual-mean net heating of the atmosphere must be balanced by the divergence of F'. We define R_f as the local TOA radiative forcing; λ as the local net radiative feedback, meaning the change in the net TOA radiative flux per degree of local surface warming (W m^{-2} K^{-1}); and G' as the change in net surface heat flux or ocean heat uptake. Combining these three terms with the divergence of Equation 1 gives

$$R_f + \lambda T' - G' = \nabla \cdot F', \tag{2}$$

which is a single differential equation that can be solved numerically for T' and F' given zonal-mean profiles of R_f, G', and λ and a value (or zonal-mean profile) of D. Figure S1 in Supporting Information S1 shows the zonal-mean pattern of T' from each CMIP5 model and MEBM solution. For the multi-model mean analysis, we set $D = 1.02 \times 10^6$ m^2 s^{-1}, which is the multi-model mean value from pre-industrial control (piControl) simulations (see Section 2.2). For the individual model analyses, D is unique to each climate model. Supporting Information S1 provides more detail as to how D is calculated.

Following Siler et al. (2018), we simulate the change in poleward latent energy transport F'_{latent} as the sum of two components that represent transport by the Hadley Cells and transport by midlatitude eddies. To correctly simulate equator-ward latent energy transport in the tropics, we use a simple Hadley Cell parameterization to approximate the Hadley Cell mass flux ψ (kg s^{-1}). The strength of ψ is found by partitioning poleward atmospheric energy transport into a component due to midlatitude eddies and a component due to the Hadley Cell using a Gaussian weighting function w and energetic constraints on gross moist stability (see Siler et al. (2018) and Supporting Information S1 for more details). For the midlatitude eddies, latent energy transport is parameterized as downgradient diffusion modulated by w. The total change in poleward latent energy transport is thus

$$F'_{\text{latent}} = \underbrace{-(\psi' L_v \bar{q} + \bar{\psi} L_v q' + \psi' L_v q')}_{\text{Hadley Cells}} - \underbrace{(1 - w) \frac{2\pi p_s}{g} L_v D (1 - x^2) \frac{dq'}{dx}}_{\text{Eddies}}, \tag{3}$$

where $\overline{(\cdot)}$ denotes the climatological control state and $(\cdot)'$ denotes the change under warming. Supporting Information S1 details how the climatological state of each climate model is approximated with the MEBM. The zonal-mean pattern of $P' - E'$ can be found by taking the divergence of Equation 3 and is shown for each climate model in Figure S2 in Supporting Information S1. Combining the divergence of Equation 3 with Equation 2 and rearranging gives

$$P' - E' = G' - R_f - \lambda T' + \nabla \cdot F'_{\text{dry}}, \tag{4}$$

where $\nabla \cdot F'_{\text{dry}}$ is the change in dry-static energy flux divergence. The MEBM F'_{dry} is computed as the residual between the atmospheric energy transport (Equation 1) and the latent energy transport (Equation 3). The dry-static energy transport can be further decomposed into a thermodynamic term and a dynamic term, where the dynamic term accounts for changes in the Hadley circulation. Equation 4 relates zonal-mean $P - E$ change directly to the atmospheric energy budget in the spirit of Muller and O'Gorman (2011), except now the representation of ocean heat uptake is explicit because Equation 2 represents TOA radiative feedbacks and radiative forcing. Crucially, in this framework, the zonal-mean pattern of $P' - E'$ can change depending on the zonal-mean pattern of R_f, G', λ, and T' both through local energetic constraints and nonlocal changes in atmospheric energy transport and feedback interactions.

2.2. CMIP5 Output

In this study, we use monthly mean output from 27 CMIP5 models (see Table S1 in Supporting Information S1 for more information). We use the r1i1p1 ensemble from the piControl and abrupt CO2 quadrupling (abrupt4xCO2) simulations and calculate time-averaged anomalies for years 120–150 in the abrupt4xCO2 simulations relative to the concurrent piControl climatology.

We use zonal-mean patterns of λ from Feldl et al. (2020), which were calculated using the radiative-kernel method (Shell et al., 2008; Soden & Held, 2006; Soden et al., 2008) with CESM1-CAM5 radiative kernels (Pendergrass et al., 2018). The feedbacks are presented here using the decomposition described by Held and Shell (2012) which includes the water vapor changes that occur at constant relative humidity in the lapse rate and Planck feedbacks, and a separate relative-humidity feedback associated with changes in relative humidity. Each feedback is found by taking the difference in the climate variable between the piControl and abrupt4xCO2 simulations and multiplying the variable by the respective radiative kernel. We calculate the zonal-mean pattern of R_f as the y-intercept of the regression between TOA radiation anomalies at each grid point against the global-mean near-surface temperature anomalies for the first 20 years after abrupt4xCO2 (Gregory et al., 2004). Smith et al. (2020) noted that this 20-year regression produces radiative forcing values that closely match methods using fixed sea-surface temperatures (Hansen et al., 2005). Finally, we calculate the zonal-mean pattern of G' as anomalies in the net surface heat flux relative to the piControl simulations. Figure S3 in Supporting Information S1 shows the zonal-mean profiles of λ, R_f and G' for each climate model.

2.3. Global Climate Model (GCM) Experiments

We analyze a set of locked cloud feedback simulations from Chalmers et al. (2022) using the CESM1-CAM5 (Hurrell et al., 2013). Two pairs of simulations are used. In the first pair, CO_2 concentrations are abruptly doubled (abrupt2xCO2) from the 1850 piControl levels and held constant for 150 years. The second pair of simulations are a repeat of the first pair but with cloud radiative feedbacks disabled (Chalmers et al., 2022; Middlemas et al., 2020). Cloud feedbacks are disabled by prescribing cloud radiative properties from a neutral El Niño/Southern Oscillation preindustrial year in the atmospheric model radiation calculations, while leaving the rest of the climate system to freely evolve. Note that the cloud-locked pair contains a cloud-locked piControl simulation that is used as a reference climate state.

For each variable, we compute climatological averages from the years 100–150 of each abrupt2xCO2 simulation and compare this to the concurrent piControl climatology centered on years 100–150. The zonal-mean patterns of λ and G' are calculated using a similar procedure as described above. However, the zonal-mean pattern of R_f is calculated from abrupt2xCO2 simulations under fixed-SST conditions (Smith et al., 2020).

3. Influence of Climate Feedbacks on Regional Hydrological Change

We begin by examining the influence of individual feedbacks on regional $P - E$ change by systematically locking each in the MEBM. Below, we describe the process of feedback locking in the MEBM. While the contribution of radiative feedbacks to regional $P - E$ can be inferred directly from an atmospheric energy budget (e.g., Bonan, Feldl, et al., 2023), such diagnostic approaches miss interactions between feedbacks and atmospheric energy transport (e.g., Beer & Eisenman, 2022). The feedback locking approach alleviates these concerns by turning off individual feedbacks and allowing the climate system to adjust, thus quantifying the full influence of a particular feedback. This approach also allows us to improve on Muller and O'Gorman (2011) and examine how radiative feedbacks affect dry-static energy transport and thus indirectly affect regional $P - E$ change.

3.1. Feedback Locking

The net feedback λ is the sum of individual feedbacks

$$\lambda = \sum_i \lambda_i, \tag{5}$$

where i is the index of the individual feedback. To lock each feedback, we replace λ with $\lambda - \lambda_i$ in the MEBM. We refer to the resulting pattern of T' as T'_{-i} and $P' - E'$ as $(P' - E')_{-i}$. Similarly, because the locked feedback simulation also results in a change in atmospheric energy transport, we refer to the resulting change in atmospheric energy transport as F'_{-i} or $F'_{\text{dry},-i}$ and $F'_{\text{latent},-i}$ for the dry-static and latent energy transport changes, respectively. Note that in this MEBM, G' and R_f cannot change in a locked feedback simulation. This assumption is further examined in Section 3.4. With these terms, the hydrological component of the MEBM when a feedback is locked can be written as

$$(P' - E')_{-i} = G' - R_f - (\lambda - \lambda_i) \, T'_{-i} + \nabla \cdot F'_{\text{dry},-i}. \tag{6}$$

The pattern of T' and $P' - E'$ attributed to each feedback process in this approach, T'_i and $(P' - E')_i$, can be found by taking the difference between the MEBM with all feedbacks active (Equation 4) and the MEBM with an individual feedback locked (Equation 6) as $T'_i \equiv T' - T'_{-i}$ and $(P' - E')_i \equiv (P' - E') - (P' - E')_{-i}$. A similar procedure can be done to isolate the influence of G' and R_f on T' and $P' - E'$. Figure S4 in Supporting Information S1 shows how each term in Equation 2 contributes to the pattern of T' and $P' - E'$. For the remainder of the analysis, we focus on the surface-albedo, relative-humidity, lapse-rate, and net cloud feedbacks. We do not analyze the Planck feedback as removing it from the MEBM causes stability issues but note that Bonan, Feldl, et al. (2023) found the Planck feedback exerts a strong influence on regional precipitation change in the high-latitudes.

Figure 1 shows the impact of removing each (left) individual feedback on (middle) zonal-mean T' and (right) zonal-mean $P' - E'$. Overall, the influence of each feedback on zonal-mean T' and $P' - E'$ is regionally distinct. When the surface-albedo feedback is removed, warming in both the Arctic and Antarctic is substantially reduced and warming in the subtropics and deep tropics is approximately the same (Figure 1a, middle). In contrast, the $P - E$ changes associated with the surface-albedo feedback has similar magnitudes in the tropics and polar regions (Figure 1a, right). There is also a shift in tropical $P' - E'$ with increasing $P - E$ around 10°N and decreasing $P - E$ around 10°S. This is consistent with high-latitude albedo changes resulting in meridional shifts in the location of the ITCZ (e.g., Chiang & Bitz, 2005).

The impact of removing other feedbacks on T' and $P' - E'$ is even more striking. The relative-humidity feedback contributes to global cooling that is nearly uniform in latitude (Figure 1b, middle). The resulting zonal-mean pattern of $P' - E'$ results in dry regions (like the subtropics) getting slightly wetter and wet regions (like the extratropics) getting slightly drier, though the magnitude is quite weak, with the maximum $P - E$ change being approximately 0.05 mm day^{-1} (Figure 1b, right). The lapse-rate feedback contributes to a small amount of surface warming in the Arctic and surface cooling at most other latitudes (Figure 1c, middle). The $P - E$ change associated with the lapse-rate feedback also results in dry regions (like the subtropics) getting slightly wetter and wet regions (like the extratropics) getting slightly drier (Figure 1c, right). Notably, the lapse-rate feedback modulates the amplitude of the hydrological cycle largely through its control on global-mean warming (Figure 1c, middle). The cloud feedback, on the other hand, contributes to warming everywhere of approximately 1°C, except for the Antarctic, where it contributes to slight cooling of approximately 0.5°C (Figure 1d, middle). The zonal-mean pattern of $P' - E'$, however, exhibits distinct regional features. Here the cloud feedback is associated with an increase in $P - E$ in the deep tropics and a narrowing of the change in the ITCZ region, which can be seen as an equator-ward shift of where $P' - E' = 0$. This is consistent with previous work arguing that ITCZ biases are related to cloud radiative biases (e.g., Hwang & Frierson, 2013). The cloud feedback also contributes slightly to an increase in $P - E$ in the high latitudes of each hemisphere, including the peak increase in $P - E$ over the Southern Ocean (Figure 1d, right).

3.2. Decomposition of Regional Hydrological Change

The influence of an individual feedback on $P - E$ changes can be attributed to three terms: (a) the $P - E$ change due to the feedback in isolation, (b) the $P - E$ change due to interactions between the feedback and other climate feedbacks, and (c) the $P - E$ change due to interactions between the feedback and dry-static energy transport. The contributions of these three terms can be identified by subtracting the equation for the MEBM with a feedback locked (Equation 6) from the equation for the full MEBM (Equation 4). Further simplification of these terms can be found by rewriting the net feedback given by Equation 5 as $\lambda = \lambda_i + \sum_{j \neq i} \lambda_j$ and using the definition of T'_i in Section 3.1. This results in

$$(P' - E')_i = \underbrace{- \lambda_i T'}_{(1)} \underbrace{- \sum_{j \neq i} \lambda_j T'_i}_{(2)} + \underbrace{(\nabla \cdot F'_{\text{dry}} - \nabla \cdot F'_{\text{dry},-i})}_{(3)}. \tag{7}$$

The left-hand side of Equation 7 represents the $P - E$ change associated with an individual feedback i in the feedback locking analysis. The three terms on the right hand side of Equation 7 represent the $P - E$ change
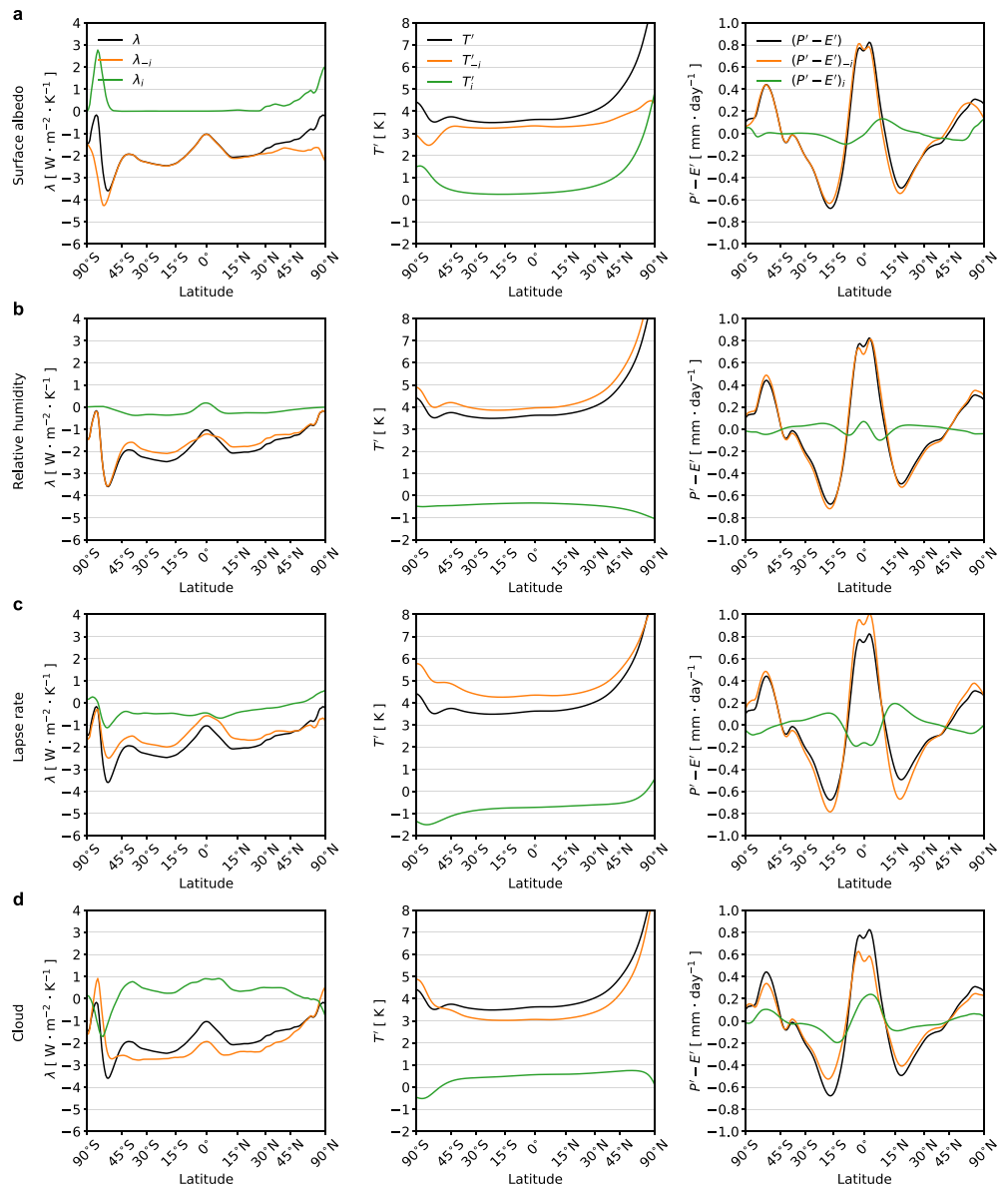
Figure 1. Influence of climate feedbacks on regional hydrological changes. Contribution of the (a) surface-albedo feedback, (b) relative-humidity feedback, (c) lapse-rate feedback, and (d) shortwave and longwave cloud feedbacks to changes in zonal-mean temperature (T') and precipitation minus evaporation ($P' - E'$). The left panel shows the (black) net feedback, (orange) net feedback with the individual feedback removed, and (green) individual feedback. The middle panel shows the pattern of T' associated with the (black) net feedback and (orange) individual feedback removed from the net feedback. The green line represents the impact of the individual feedback on T' and is found by taking the difference between the black line and the orange line. The right panel shows same but for the pattern of $P' - E'$. All panels are shown the CMIP5 multi-model mean.

associated with: (a) the individual feedback; (b) the product of all other feedbacks and the warming associated with the inclusion of feedback i; and (c) changes in the dry-static energy flux divergence induced by the inclusion of feedback i. A similar expression can be derived for temperature change as detailed in Beer and Eisenman (2022).

Figure 2 shows the three terms in Equation 7 for each feedback as well as the thermodynamic and dynamic contributions to the dry-static energy flux divergence. For the surface-albedo feedback, the increase in tropical $P - E$ and shift of the ITCZ is related to the dynamical change in the dry-static energy flux divergence (Figure 3a,
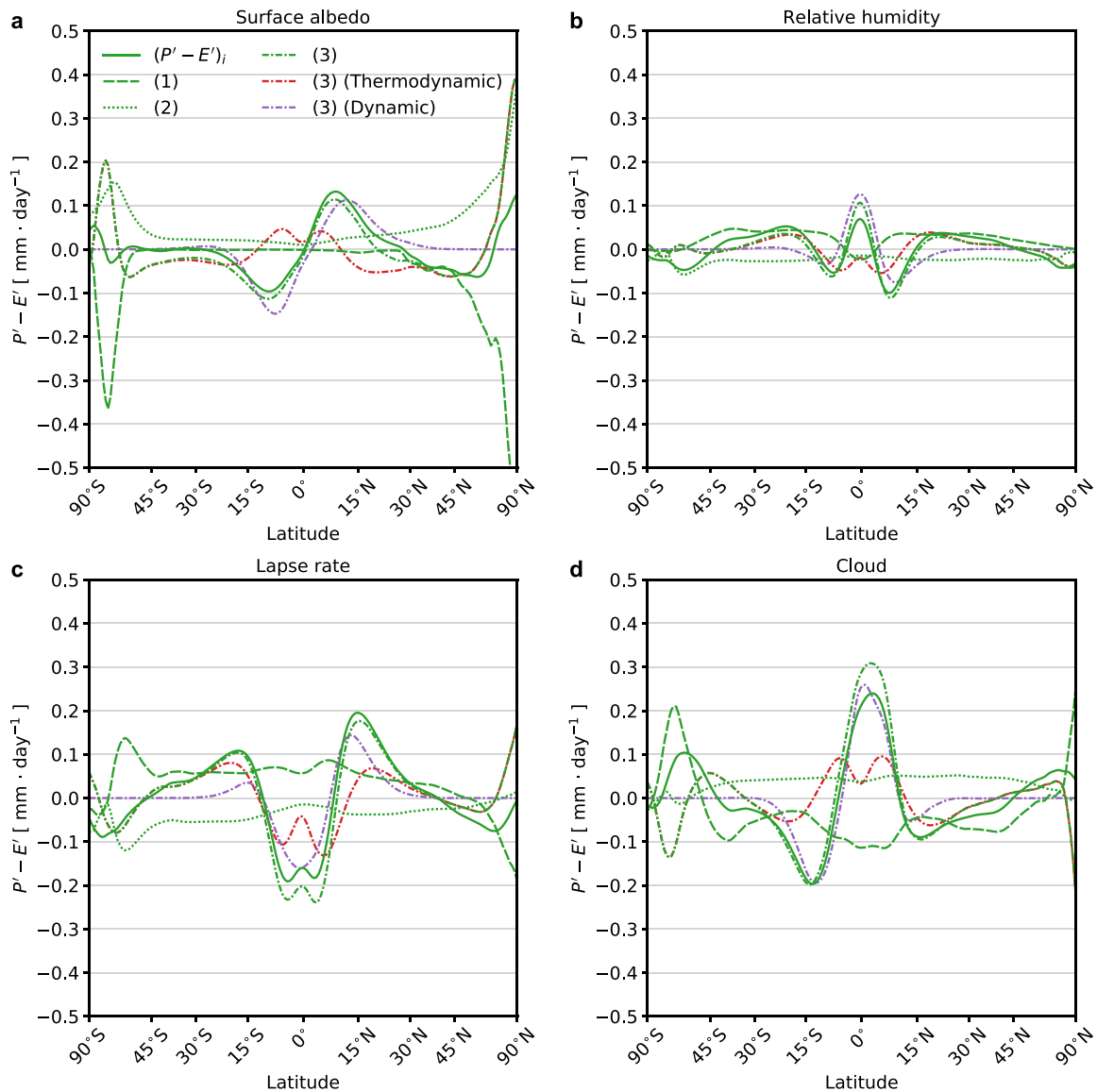
Figure 2. Decomposition of regional hydrological changes for each climate feedback. Contribution of the (a) surface-albedo feedback, (b) relative-humidity feedback, (c) lapse-rate feedback, and (d) shortwave and longwave cloud feedbacks to (green) changes in zonal-mean precipitation minus evaporation ($P' - E'$) decomposed into three terms. Term 1 (dash) represents the individual contribution of the feedback alone, Term 2 (dot) represents interactions with other feedbacks, and Term 3 (dash-dot) represents dry-static energy transport changes. Term 3 (dash-dot) is further broken up into thermodynamic (red) and dynamic (purple) components. The three green dash/dot green lines sum to the solid green line. All panels are shown the CMIP5 multi-model mean.

purple line). As noted by Bonan, Siler, et al. (2023), the Hadley Cell mass flux change can be decomposed into changes associated with the poleward atmospheric energy transport and changes in gross moist stability. The change in poleward energy transport dominates the Hadley Cell mass flux change for all feedback-locking simulations (not shown). In the high latitudes, the surface-albedo feedback in isolation results in a large decrease in $P - E$ that is compensated by a large increase in $P - E$ from other feedbacks (dotted) and the dry-static energy flux divergence (dash-dot). The surface-albedo feedback contributes to strong polar amplification (Figure 1a, middle) which reduces the dry-static energy flux convergence in the polar regions and is associated with a cooling tendency that is balanced by an increase in latent heat release associated with an increase in $P - E$.

The other feedbacks also have regionally distinct patterns associated with distinct mechanisms. For the relative-humidity feedback, the increase in subtropical $P - E$ is almost entirely related to the thermodynamic dry-static
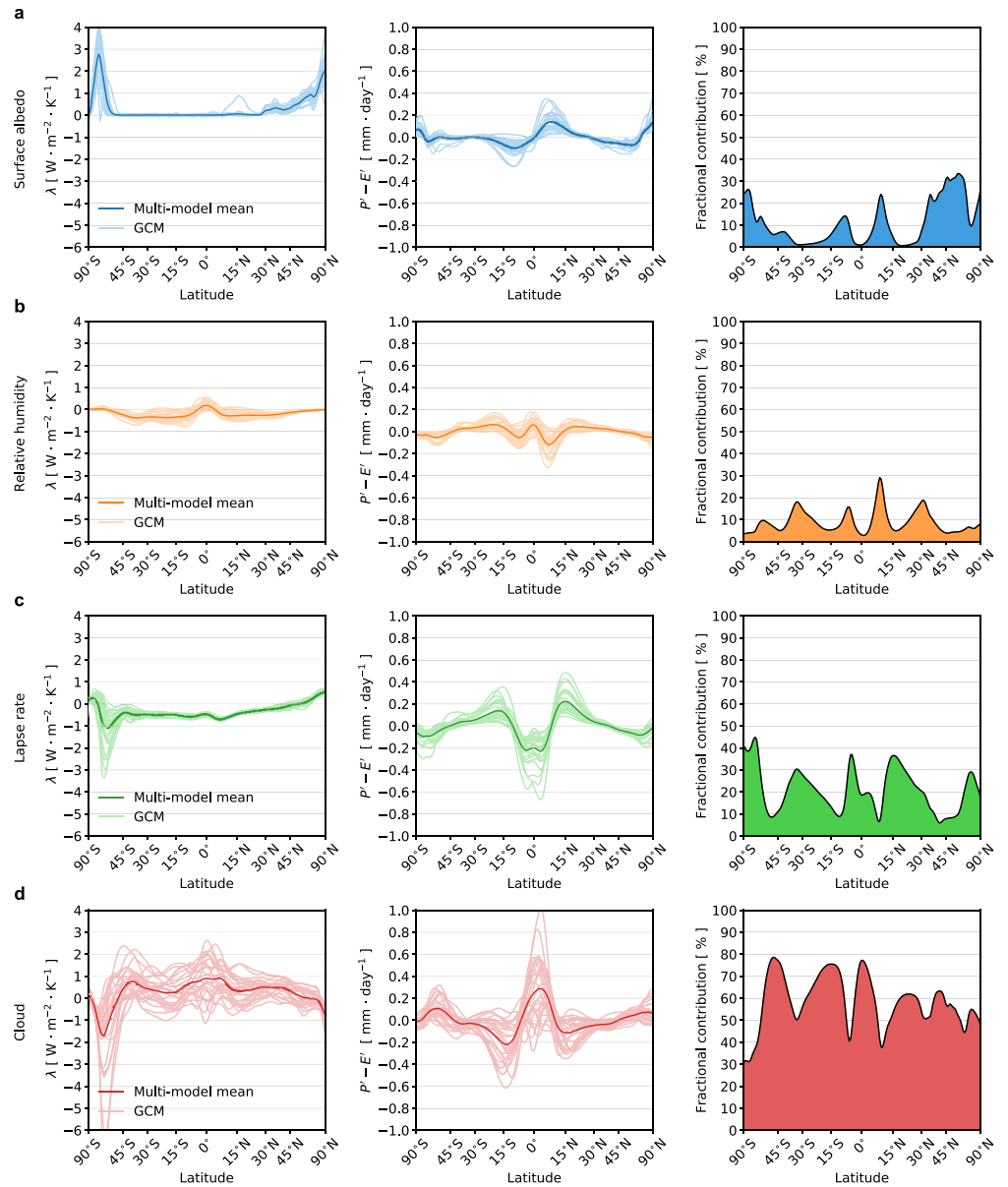
Figure 3. Contribution of climate feedbacks to the intermodel spread in regional hydrological changes. The left panel shows the (a) surface-albedo feedback, (b) relative-humidity feedback, (c) lapse-rate feedback, and (d) shortwave and longwave cloud feedbacks for 27 CMIP5 models. The middle panel shows the zonal profile of $P' - E'$ associated with each feedback (a)–(e). The light colored lines denote individual climate models and the dark lines denote the multi-model mean. The right panel shows the fractional contribution of each feedback to the total uncertainty in $P - E$ change for these four feedbacks.

energy flux divergence and the relative-humidity feedback in isolation. For the lapse-rate feedback, every term in Equation 7 contributes to the overall structure of $P - E$ change. In the deep tropics and subtropics, the decrease in $P - E$ is contributed equally by both the dynamic and thermodynamic dry-static energy flux divergence change. However, in the polar regions, the lapse-rate feedback in isolation is associated with a decrease in $P - E$ which is somewhat compensated by an increase in $P - E$ from dry-static energy flux divergence. This is also consistent with Bonan, Feldl, et al. (2023) who found the lapse-rate feedback is associated with a decrease in high-latitude precipitation. For the cloud feedback, the narrowing of the ITCZ and $P - E$ change in the tropics and subtropics is almost entirely related to the dynamical change in the dry-static energy flux divergence. Here, the cloud feedback causes the net feedback to be much less negative in the deep tropics. This limits the atmosphere from radiating energy to space locally, and means it must transport this energy to the subtropics, where radiative loss is more

efficient due to a strongly negative net feedback. This increase in transport requires an increase in the Hadley Cell mass flux and increases $P - E$ in the deep tropics. This is also consistent with Merlis (2015) and Byrne and Schneider (2016), who argued local energetic constraints can explain large-scale Hadley circulation changes and ITCZ changes. Finally, in the polar regions, such as the Southern Ocean, the cloud feedback in isolation is associated with most of the $P - E$ change.

3.3. Sources of Uncertainty

The large influence of individual climate feedbacks on the pattern of $P - E$ change suggests that individual feedbacks also influence the intermodel spread in $P - E$ change. To quantify the contributions of individual feedbacks to the intermodel spread in $P - E$ change, we run the MEBM with individual feedbacks locked for each of the 27 CMIP5 models and subtract the feedback-locked simulation from the full-feedback simulation as detailed in Section 3.1. Figure 3 shows (left) the intermodel spread of each individual feedback, (middle) the resulting change in $(P' - E')_i$, and (right) the fractional contribution of each feedback to the total feedback variance in $P' - E'$. We approximate the variance from each feedback as a linear sum such that the fractional contribution of all feedbacks sums to one.

Overall, each feedback contributes substantially to the intermodel spread in regional $P - E$ change. The surface-albedo feedback, despite being confined mainly to the polar regions, contributes to tropical and subtropical uncertainty in $P - E$ change, accounting for 10%–20% of the total intermodel variance for these four feedbacks (Figure 3a, right). However, the influence of intermodel variations in the surface-albedo feedback on $P - E$ change is largest in the polar regions, accounting for 20%–35% of the total variance for these four feedbacks. The relative-humidity feedback contributes nearly uniform uncertainty with some larger influence in the subtropical regions (Figure 3b, right). Intermodel variations in the lapse-rate feedback lead to large intermodel variations in $P - E$ change in the deep tropics, subtropics, and high-latitude regions. In the polar regions, the surface-albedo and lapse-rate feedback combined contribute to approximately 60% of the total variance for these four feedbacks (Figures 3a–3c). However, intermodel variations in the cloud feedback dominate uncertainty in $P - E$ change, contributing approximately 60% of the total variance for these four feedbacks globally (Figure 3d). And at some latitudes, the cloud feedback contributes more than 70% of the total variance for these four feedbacks in $P - E$ change.

3.4. GCM and MEBM Comparison

Our feedback locking approach allowed us to isolate the impact of individual feedback processes on regional hydrological changes within the MEBM. However, because the MEBM does not allow for the feedbacks to influence other components, it is worth considering the extent to which its results hold within comprehensive climate models. Numerous studies have locked cloud, surface-albedo, and water-vapor feedbacks in coupled climate models (Chalmers et al., 2022; Graversen & Wang, 2009; Hall, 2004; Langen et al., 2012; Mauritsen et al., 2013; Middlemas et al., 2020; Voigt et al., 2019; Wetherald & Manabe, 1988). These studies have all found that when one feedback is locked other components of the climate system change, suggesting the MEBM might be too simple to quantify the influence of feedbacks on $P - E$ change. To assess the limitation of the MEBM framework we compare the cloud feedback locking experiments in the MEBM with cloud feedback locking experiments in CESM1-CAM5, using the simulations from Chalmers et al. (2022).

The left panel of Figure 4a shows the CESM1-CAM5 net radiative feedback from the standard abrupt2xCO2 simulation (black line) and abrupt2xCO2 simulation with locked cloud radiative effects (orange line). With cloud-locking, the net feedback becomes more negative at most latitudes except in the Southern Ocean (orange line, left panel, Figure 4a). The zonal-mean temperature change from the cloud-locked abrupt2xCO2 simulation is less at all latitudes, particularly in the Arctic, when compared to the normal abrupt2xCO2 simulation (compare black and orange line, middle panel, Figure 4a). Thus, the radiative effects of clouds results in warming at all latitudes with stronger Arctic warming (green line, middle panel, Figure 4a). The $P - E$ change, however, is quite distinct with and without cloud locking. With cloud-locking, there is a large decrease in $P - E$ near the southern edge of the ITCZ and large decreases in $P - E$ in the extratropics of each hemisphere when compared to the normal abrupt2xCO2 simulation (compare black and orange line, right panel, Figure 4a). This suggests cloud radiative effects act to increase $P - E$ at the southern edge of the ITCZ and in the extratropics of each hemisphere, and decrease $P - E$ at the northern edge of the ITCZ (green line, right panel, Figure 4a).
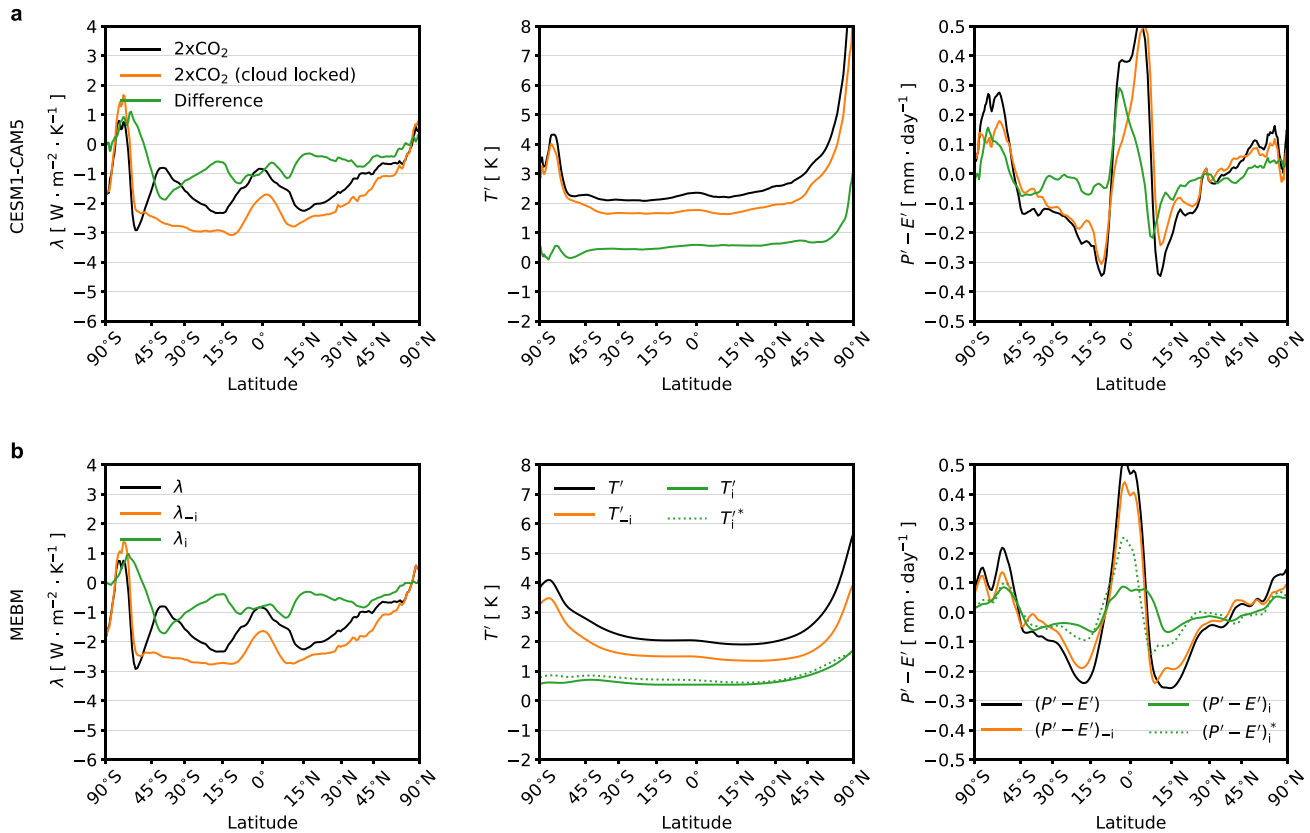
Figure 4. Feedback locking in a GCM and a MEBM. (a) The zonal-mean profile of (left) λ, (middle) T', and (right) $P' - E'$ averaged $100 - 150$ years after the abrupt2xCO2 in the GCM. The black line denotes the total change and the orange line denotes the change when the cloud radiative effect has been disabled (see Section 2.3). The green line represents the impact of the cloud radiative feedback and is found by taking the difference between the black and orange line. (b) The zonal-mean profiles as in (a) but from a MEBM where the cloud radiative feedback was removed. The black line denotes the total change and the orange line denotes the change when the net cloud feedback is removed. The green line in the left panel of (b) represents the net cloud feedback diagnosed from the simulation with interactive clouds. The green dotted lines in (b) denote the MEBM solutions for T' and $P' - E'$ with λ, G', and R_f from the cloud-locked GCM simulation.

Locking cloud feedbacks and then doubling CO_2 results in a similar net feedback pattern to doubling CO_2 and removing the net cloud feedback diagnosed from the simulation with interactive clouds (compare orange line, Figures 4a and 4b, left). Note that the feedback patterns differ slightly in the Southern Hemisphere subtropics. However, despite similarity in the net radiative feedback, the MEBM patterns of T' and $P' - E'$ are slightly different from the GCM-based results (compare orange lines, Figures 4a and 4b, middle/right). For T', when the cloud feedback is removed, the MEBM predicts less warming, similar to CESM1, but does not simulate the correct magnitude of Arctic warming. For $P' - E'$, when the cloud feedback is removed, the MEBM correctly simulates the decrease in $P - E$ in the extratropics of each hemisphere but fails to simulate the shift in tropical $P - E$. A possible reason for these discrepancies comes from the fact that G' and R_f also change in the CESM1-based cloud-locking simulation, resulting in slightly less Northern Hemisphere ocean heat uptake and weaker radiative forcing (see Figure S5 in Supporting Information S1). When the patterns of G', R_f, and λ from the cloud-locked abrupt2xCO2 simulation are prescribed, the MEBM more correctly simulates the zonal-mean pattern of T' and $P' - E'$ change (green dotted line Figure 4b, middle/right).

In summary, the MEBM-based feedback locking approximates the CESM1-based feedback locking well in the extratropics, but less well in the tropics. However, the MEBM still predicts the correct tropical hydrological change when the patterns of G' and R_f are included, which is consistent with the requirements from atmospheric energy transport changes. Overall, we conclude that the principle of down-gradient energy transport by the atmosphere provides valuable intuition for how climate feedbacks influence regional hydrological change.

4. Discussion and Conclusions

In this study, we examined how radiative feedbacks influence the response of zonal-mean $P - E$ to global warming by explicitly accounting for interactions among feedbacks and atmospheric energy transport in a MEBM with a Hadley Cell parameterization. We systematically locked individual radiative feedbacks in the MEBM and showed how each feedback can substantially modulate the so-called "wet-gets-wetter, dry-get-drier" paradigm commonly applied to understanding the response of $P - E$ to greenhouse-gas forcing.

Overall, $P - E$ change in the tropics and subtropics is influenced by changes in the dry-static energy flux divergence, while $P - E$ change in the polar regions is influenced by both changes in the dry-static energy flux divergence and radiative feedbacks—consistent with Bonan, Feldl, et al. (2023). However, the contribution of radiative feedbacks to regional $P - E$ change is more nuanced than previously thought, as radiative feedbacks can significantly alter dry-static energy transport and thus indirectly influence regional $P - E$ change (see Equation 7). For example, we found that the surface-albedo feedback can shift the location of maximum tropical $P - E$ change by changing the Hadley circulation. We also found that the cloud feedback acts to narrow bands of tropical $P - E$ and increase tropical $P - E$ by causing an export of energy from the deep tropics. This causes the Hadley Cell mass flux to increase and $P - E$ in the deep tropics to increase via increased equatorward moisture transport. Finally, we showed that the lapse-rate feedback contributes to a decrease in $P - E$ in the polar regions, which is similar to the thermodynamic contributions described in Siler et al. (2023) and the energy budget analysis described in Bonan, Feldl, et al. (2023).

While we showed that radiative feedbacks strongly influence the spatial pattern of $P - E$ change, our study has an important caveat: the radiative feedbacks in the MEBM cannot influence other components such as G' or R_f. It is clear that this assumption affects subtropical and tropical $P - E$ change associated with the net cloud feedback. When compared to the cloud-locked GCM (CESM1-CAM5), the MEBM with a cloud feedback removed does not capture the full shift of the ITCZ. But when the MEBM also contains the cloud-locked patterns of G' and R_f, the structure of $P - E$ change aligns much better with the GCM. While the MEBM accounts for interactions across the radiative responses of the feedbacks (Term 2, Equation 7), it does not include changes in the feedback processes themselves or interactions with G' or R_f. Including the ability for other components to change when an individual feedback is locked might better align the MEBM with GCM-based result. Nonetheless, the fact the MEBM largely replicates the $P' - E'$ pattern of the cloud-locked GCM simulation, particularly in the extratropics, suggests downgradient energy transport can provide valuable intuition for understanding how radiative feedbacks influence the patterns of climate change.

Overall, these results demonstrate how the spatial structure of radiative feedbacks influence zonal-mean $P - E$ change and can cause significant deviations from the "wet-gets-wetter, dry-gets-drier" thermodynamic paradigm. Key results from this analysis are that under greenhouse-gas forcing, cloud feedbacks act to narrow the ITCZ and increase $P - E$ in the deep tropics, and the surface-albedo feedback acts to shift the ITCZ and increase $P - E$ in the polar regions. We further find that cloud feedbacks dominate feedback uncertainty in $P - E$ change for most regions, except in the polar regions where the surface-albedo feedback and lapse-rate feedbacks dominate feedback uncertainty in $P - E$ change.

Data Availability Statement

The authors thank the climate modeling groups for producing and making available their model output, which is accessible at the Earth System Grid Federation (ESGF) Portal (https://esgf-node.llnl.gov/search/cmip5/). A list of the CMIP5 models used in this study is provided in Table S1 in Supporting Information S1. The processed model output and code for the moist energy balance model is available at Bonan (2024).

References

Anderson, B. T., Feldl, N., & Lintner, B. R. (2018). Emergent behavior of Arctic precipitation in response to enhanced Arctic warming. *Journal of Geophysical Research: Atmospheres*, *123*(5), 2704–2717. https://doi.org/10.1002/2017jd026799

Armour, K. C., Siler, N., Donohoe, A., & Roe, G. H. (2019). Meridional atmospheric heat transport constrained by energetics and mediated by large-scale diffusion. *Journal of Climate*, *32*(12), 3655–3680. https://doi.org/10.1175/jcli-d-18-0563.1

Beer, E., & Eisenman, I. (2022). Revisiting the role of the water vapor and lapse rate feedbacks in the Arctic amplification of climate change. *Journal of Climate*, *35*(10), 2975–2988. https://doi.org/10.1175/jcli-d-21-0814.1

Bonan, D. B. (2024). Dave-bonan/energy-balance-models: Moist EBM for Bonan et al., (2024, GRL) (v1.1). [Software]. Zenodo. https://doi.org/10.5281/zenodo.10565268

Bonan, D. B., Armour, K., Roe, G., Siler, N., & Feldl, N. (2018). Sources of uncertainty in the meridional pattern of climate change. *Geophysical Research Letters*, *45*(17), 9131–9140. https://doi.org/10.1029/2018gl079429

Bonan, D. B., Feldl, N., Zelinka, M. D., & Hahn, L. C. (2023a). Contributions to regional precipitation change and its polar-amplified pattern under warming. *Environmental Research: Climate*, *2*(3), 035010. https://doi.org/10.1088/2752-5295/ace27a

Bonan, D. B., Siler, N., Roe, G., & Armour, K. (2023b). Energetic constraints on the pattern of changes to the hydrological cycle under global warming. *Journal of Climate*, *36*(10), 3499–3522. https://doi.org/10.1175/jcli-d-22-0337.1

Byrne, M. P., & Schneider, T. (2016). Narrowing of the ITCZ in a warming climate: Physical mechanisms. *Geophysical Research Letters*, *43*(21), 11–350. https://doi.org/10.1002/2016gl070396

Cess, R. D., & Potter, G. L. (1987). Exploratory studies of cloud radiative forcing with a general circulation model. *Tellus*, *39*(5), 460–473. https://doi.org/10.1111/j.1600-0870.1987.tb00321.x

Cess, R. D., Potter, G. L., Blanchet, J., Boer, G., Ghan, S., Kiehl, J., et al. (1989). Interpretation of cloud-climate feedback as produced by 14 atmospheric general circulation models. *Science*, *245*(4917), 513–516. https://doi.org/10.1126/science.245.4917.513

Chalmers, J., Kay, J. E., Middlemas, E. A., Maroon, E. A., & DiNezio, P. (2022). Does disabling cloud radiative feedbacks change spatial patterns of surface greenhouse warming and cooling? *Journal of Climate*, *35*(6), 1787–1807. https://doi.org/10.1175/jcli-d-21-0391.1

Charney, J. G., Arakawa, A., Baker, D. J., Bolin, B., Dickinson, R. E., Goody, R. M., et al. (1979). Carbon dioxide and climate: A scientific assessment. *National Academy of Sciences*.

Chiang, J. C., & Bitz, C. M. (2005). Influence of high latitude ice cover on the marine intertropical convergence zone. *Climate Dynamics*, *25*(5), 477–496. https://doi.org/10.1007/s00382-005-0040-5

Dufresne, J.-L., & Bony, S. (2008). An assessment of the primary sources of spread of global warming estimates from coupled atmosphere–ocean models. *Journal of Climate*, *21*(19), 5135–5144. https://doi.org/10.1175/2008jcli2239.1

Feldl, N., Bordoni, S., & Merlis, T. M. (2017). Coupled high-latitude climate feedbacks and their impact on atmospheric heat transport. *Journal of Climate*, *30*(1), 189–201. https://doi.org/10.1175/jcli-d-16-0324.1

Feldl, N., & Merlis, T. M. (2021). Polar amplification in idealized climates: The role of ice, moisture, and seasons. *Geophysical Research Letters*, *48*(17), e2021GL094130. https://doi.org/10.1029/2021gl094130

Feldl, N., Po-Chedley, S., Singh, H. K., Hay, S., & Kushner, P. J. (2020). Sea ice and atmospheric circulation shape the high-latitude lapse rate feedback. *NPJ Climate and Atmospheric Science*, *3*(1), 1–9. https://doi.org/10.1038/s41612-020-00146-7

Flannery, B. P. (1984). Energy balance models incorporating transport of thermal and latent energy. *Journal of the Atmospheric Sciences*, *41*(3), 414–421. https://doi.org/10.1175/1520-0469(1984)041<0414:ebmito>2.0.co;2

Goosse, H., Kay, J. E., Armour, K. C., Bodas-Salcedo, A., Chepfer, H., Docquier, D., et al. (2018). Quantifying climate feedbacks in polar regions. *Nature Communications*, *9*(1), 1919. https://doi.org/10.1038/s41467-018-04173-0

Graversen, R. G., & Wang, M. (2009). Polar amplification in a coupled climate model with locked albedo. *Climate Dynamics*, *33*(5), 629–643. https://doi.org/10.1007/s00382-009-0535-6

Gregory, J., Ingram, W., Palmer, M., Jones, G., Stott, P., Thorpe, R., et al. (2004). A new method for diagnosing radiative forcing and climate sensitivity. *Geophysical Research Letters*, *31*(3). https://doi.org/10.1029/2003gl018747

Hahn, L. C., Armour, K. C., Zelinka, M. D., Bitz, C. M., & Donohoe, A. (2021). Contributions to polar amplification in CMIP5 and CMIP6 models. *Frontiers in Earth Science*, *9*, 710036. https://doi.org/10.3389/feart.2021.710036

Hall, A. (2004). The role of surface albedo feedback in climate. *Journal of Climate*, *17*(7), 1550–1568. https://doi.org/10.1175/1520-0442(2004)017<1550:trosaf>2.0.co;2

Hansen, J., Lacis, A., Rind, D., Russell, G., Stone, P., Fung, I., et al. (1984). Climate sensitivity: Analysis of feedback mechanisms. *Climate processes and Climate Sensitivity*, *29*, 130–163. https://doi.org/10.1029/gm029p0130

Hansen, J., Sato, M., Ruedy, R., Nazarenko, L., Lacis, A., Schmidt, G., et al. (2005). Efficacy of climate forcings. *Journal of Geophysical Research*, *110*(D18), D18104. https://doi.org/10.1029/2005jd005776

Held, I. M., & Shell, K. M. (2012). Using relative humidity as a state variable in climate feedback analysis. *Journal of Climate*, *25*(8), 2578–2582. https://doi.org/10.1175/jcli-d-11-00721.1

Held, I. M., & Soden, B. J. (2006). Robust responses of the hydrological cycle to global warming. *Journal of Climate*, *19*(21), 5686–5699. https://doi.org/10.1175/jcli3990.1

Hurrell, J. W., Holland, M. M., Gent, P. R., Ghan, S., Kay, J. E., Kushner, P. J., et al. (2013). The community Earth system model: A framework for collaborative research. *Bulletin of the American Meteorological Society*, *94*(9), 1339–1360. https://doi.org/10.1175/bams-d-12-00121.1

Hwang, Y.-T., & Frierson, D. M. (2010). Increasing atmospheric poleward energy transport with global warming. *Geophysical Research Letters*, *37*(24). https://doi.org/10.1029/2010gl045440

Hwang, Y.-T., & Frierson, D. M. (2013). Link between the double-intertropical convergence zone problem and cloud biases over the Southern Ocean. *Proceedings of the National Academy of Sciences*, *110*(13), 4935–4940. https://doi.org/10.1073/pnas.1213302110

Hwang, Y.-T., Frierson, D. M., & Kay, J. E. (2011). Coupling between Arctic feedbacks and changes in poleward energy transport. *Geophysical Research Letters*, *38*(17). https://doi.org/10.1029/2011gl048546

Langen, P. L., Graversen, R. G., & Mauritsen, T. (2012). Separation of contributions from radiative feedbacks to polar amplification on an aquaplanet. *Journal of Climate*, *25*(8), 3010–3024. https://doi.org/10.1175/jcli-d-11-00246.1

Mauritsen, T., Graversen, R. G., Klocke, D., Langen, P. L., Stevens, B., & Tomassini, L. (2013). Climate feedback efficiency and synergy. *Climate Dynamics*, *41*(9–10), 2539–2554. https://doi.org/10.1007/s00382-013-1808-7

Merlis, T. M. (2014). Interacting components of the top-of-atmosphere energy balance affect changes in regional surface temperature. *Geophysical Research Letters*, *41*(20), 7291–7297. https://doi.org/10.1002/2014gl061700

Merlis, T. M. (2015). Direct weakening of tropical circulations from masked CO_2 radiative forcing. *Proceedings of the National Academy of Sciences*, *112*(43), 13167–13171. https://doi.org/10.1073/pnas.1508268112

Merlis, T. M., & Henry, M. (2018). Simple estimates of polar amplification in moist diffusive energy balance models. *Journal of Climate*, *31*(15), 5811–5824. https://doi.org/10.1175/jcli-d-17-0578.1

Middlemas, E., Kay, J., Medeiros, B., & Maroon, E. (2020). Quantifying the influence of cloud radiative feedbacks on Arctic surface warming using cloud locking in an Earth system model. *Geophysical Research Letters*, *47*(15), e2020GL089207. https://doi.org/10.1029/2020gl089207

Muller, C. J., & O'Gorman, P. (2011). An energetic perspective on the regional response of precipitation to climate change. *Nature Climate Change*, *1*(5), 266–271. https://doi.org/10.1038/nclimate1169

Pendergrass, A. G., Conley, A., & Vitt, F. M. (2018). Surface and top-of-atmosphere radiative feedback kernels for CESM-CAM5. *Earth System Science Data*, *10*(1), 317–324. https://doi.org/10.5194/essd-10-317-2018

Peterson, H. G., & Boos, W. R. (2020). Feedbacks and eddy diffusivity in an energy balance model of tropical rainfall shifts. *npj Climate and Atmospheric Science*, *3*(1), 11. https://doi.org/10.1038/s41612-020-0114-4

Pithan, F., & Jung, T. (2021). Arctic amplification of precipitation changes—The energy hypothesis. *Geophysical Research Letters*, *48*(21), e2021GL094977. https://doi.org/10.1029/2021gl094977

Pithan, F., & Mauritsen, T. (2014). Arctic amplification dominated by temperature feedbacks in contemporary climate models. *Nature Geoscience*, *7*(3), 181–184. https://doi.org/10.1038/ngeo2071

Roe, G. H., & Baker, M. B. (2007). Why is climate sensitivity so unpredictable? *Science*, *318*(5850), 629–632. https://doi.org/10.1126/science.1144735

Roe, G. H., Feldl, N., Armour, K. C., Hwang, Y.-T., & Frierson, D. M. (2015). The remote impacts of climate feedbacks on regional climate predictability. *Nature Geoscience*, *8*(2), 135–139. https://doi.org/10.1038/ngeo2346

Shell, K. M., Kiehl, J. T., & Shields, C. A. (2008). Using the radiative kernel technique to calculate climate feedbacks in NCAR's community atmospheric model. *Journal of Climate*, *21*(10), 2269–2282. https://doi.org/10.1175/2007jcli2044.1

Siler, N., Bonan, D. B., & Donohoe, A. (2023). Diagnosing mechanisms of hydrologic change under global warming in the CESM1 large ensemble. *Journal of Climate*, *36*(23), 8243–8257. https://doi.org/10.1175/jcli-d-23-0086.1

Siler, N., Roe, G. H., & Armour, K. C. (2018). Insights into the zonal-mean response of the hydrologic cycle to global warming from a diffusive energy balance model. *Journal of Climate*, *31*(18), 7481–7493. https://doi.org/10.1175/jcli-d-18-0081.1

Smith, C. J., Kramer, R. J., Myhre, G., Alterskjær, K., Collins, W., Sima, A., et al. (2020). Effective radiative forcing and adjustments in CMIP6 models. *Atmospheric Chemistry and Physics*, *20*(16), 9591–9618. https://doi.org/10.5194/acp-20-9591-2020

Soden, B. J., & Held, I. M. (2006). An assessment of climate feedbacks in coupled ocean–atmosphere models. *Journal of Climate*, *19*(14), 3354–3360. https://doi.org/10.1175/jcli3799.1

Soden, B. J., Held, I. M., Colman, R., Shell, K. M., Kiehl, J. T., & Shields, C. A. (2008). Quantifying climate feedbacks using radiative kernels. *Journal of Climate*, *21*(14), 3504–3520. https://doi.org/10.1175/2007jcli2110.1

Stuecker, M. F., Bitz, C. M., Armour, K. C., Proistosescu, C., Kang, S. M., Xie, S.-P., et al. (2018). Polar amplification dominated by local forcing and feedbacks. *Nature Climate Change*, *8*(12), 1076–1081. https://doi.org/10.1038/s41558-018-0339-y

Taylor, K. E., Stouffer, R. J., & Meehl, G. A. (2012). An overview of CMIP5 and the experiment design. *Bulletin of the American Meteorological Society*, *93*(4), 485–498. https://doi.org/10.1175/bams-d-11-00094.1

Voigt, A., Albern, N., & Papavasileiou, G. (2019). The atmospheric pathway of the cloud-radiative impact on the circulation response to global warming: Important and uncertain. *Journal of Climate*, *32*(10), 3051–3067. https://doi.org/10.1175/jcli-d-18-0810.1

Webb, M. J., Lambert, F. H., & Gregory, J. M. (2013). Origins of differences in climate sensitivity, forcing and feedback in climate models. *Climate Dynamics*, *40*(3–4), 677–707. https://doi.org/10.1007/s00382-012-1336-x

Wetherald, R., & Manabe, S. (1988). Cloud feedback processes in a general circulation model. *Journal of the Atmospheric Sciences*, *45*(8), 1397–1416. https://doi.org/10.1175/1520-0469(1988)045<1397:cfpiag>2.0.co;2

Zelinka, M. D., Myers, T. A., McCoy, D. T., Po-Chedley, S., Caldwell, P. M., Ceppi, P., et al. (2020). Causes of higher climate sensitivity in CMIP6 models. *Geophysical Research Letters*, *47*(1), e2019GL085782. https://doi.org/10.1029/2019gl085782